AGU PUBLICATIONS

Geophysical Research Letters

RESEARCH LETTER
10.1002/2017GL075389

Key Points:
- New fault forms when subduction initiates with unfavorable dipping lithospheric heterogeneities
- Uplift and subsidence on the Puysegur Ridge are related to new fault formation and maturation
- Snares Zone is caused by differences in plate coupling at shallower and deeper fault depths

Supporting Information:
- Supporting Information S1

Correspondence to:
X. Mao,
xlmao@gps.caltech.edu

Citation:
Mao, X., Gurnis, M., & May, D. A. (2017). Subduction initiation with vertical lithospheric heterogeneities and new fault formation. *Geophysical Research Letters*, *44*, 11,349–11,356. https://doi.org/10.1002/2017GL075389

Received 22 AUG 2017
Accepted 24 OCT 2017
Accepted article online 30 OCT 2017
Published online 20 NOV 2017

Subduction Initiation With Vertical Lithospheric Heterogeneities and New Fault Formation

Xiaolin Mao[1], Michael Gurnis[1], and Dave A. May[2]

[1]Seismological Laboratory, California Institute of Technology, Pasadena, CA, USA, [2]Department of Earth Sciences, University of Oxford, Oxford, UK

Abstract How subduction initiates with mechanically unfavorable lithospheric heterogeneities is important and rarely studied. We investigate this with a geodynamic model for the Puysegur Incipient Subduction Zone (PISZ) south of New Zealand. The model incorporates a true free surface, elasto-visco-plastic rheology and phase changes. Our predictions fit the morphology of the Puysegur Trench and Ridge and the deformation history on the overriding plate. We show how a new thrust fault forms and evolves into a smooth subduction interface, and how a preexisting weak zone can become a vertical fault inboard of the thrust fault during subduction initiation, consistent with two-fault system at PISZ. The model suggests that the PISZ may not yet be self-sustaining. We propose that the Snares Zone (or Snares Trough) is caused by plate coupling differences between shallower and deeper parts, the tectonic sliver between two faults experiences strong rotation, and low-density material accumulates beneath the Snares Zone.

1. Introduction

Subduction initiation is a vital phase of the plate tectonic cycle since it fundamentally alters the global force balance on tectonic plates. Numerical studies have advanced our understanding of under what circumstances and with what physical processes a new subduction zone can develop (e.g., Gurnis et al., 2004; Nikolaeva et al., 2010; Regenauer-Lieb et al., 2001; Thielmann & Kaus, 2012; Toth & Gurnis, 1998), but uncertainty still exists and key parameters related to subduction initiation remain poorly quantified mainly due to the lack of good constraints on numerical models. Subduction initiation can be either induced or spontaneous: induced subduction initiation begins with strong compression and uplift (Gurnis et al., 2004), whereas spontaneous initiation begins with rifting and subsidence (Stern, 2004). Therefore, topographic changes that result from subduction initiation can be used to distinguish different initiation modes and can potentially be used to quantify parameters that control the initiation process. While the importance of topographic change in subduction initiation has been noticed previously (Gurnis et al., 2004), applying topographic changes as a constraint on subduction initiation process at a specific subduction zone has not been addressed, as most of the early record needed to constrain the dynamics is overprinted by later deformation and volcanism for mature subduction zones, like the well-known examples of the Eocene initiation of Izu-Bonin-Marianas and Tonga-Kermadec subduction zones (Sutherland et al., 2006). On the other hand, some possible incipient subduction zones are so young (Gorringe Bank, the Owen Ridge, the Hjort Trench, and Mussau Trench) that the slab may not have yet started to bend into the mantle (Gurnis et al., 2004).

Luckily, one subduction zone overcomes these limitations: the Puysegur Incipient Subduction Zone (PISZ). The Puysegur Trench and Ridge form the northern end of the Macquarie Ridge Complex (MRC) defining the Australian-Pacific plate margin south of New Zealand (Figure 1a). Since about 20 Ma, highly oblique convergence beneath the Puysegur Ridge results in a maximum total convergence of 150–200 km at Puysegur as suggested by a Benioff zone with seismicity down to 150 km depth (Figure 1c) (Sutherland et al., 2006). Subduction-related igneous rocks, especially adakite, which is formed by the partial melting of young oceanic crust under eclogitic facies conditions, are sparsely distributed on the overriding plate at Solander Island (Reay & Parkinson, 1997). This confirms that the slab enters the mantle. The morphology of the Puysegur Ridge (Figure 1b) shows a characteristic change from uplift in the southern part, where the total convergence is less, and subsidence in the northern part, the Snares Zone (or Snares Trough), where the total convergence

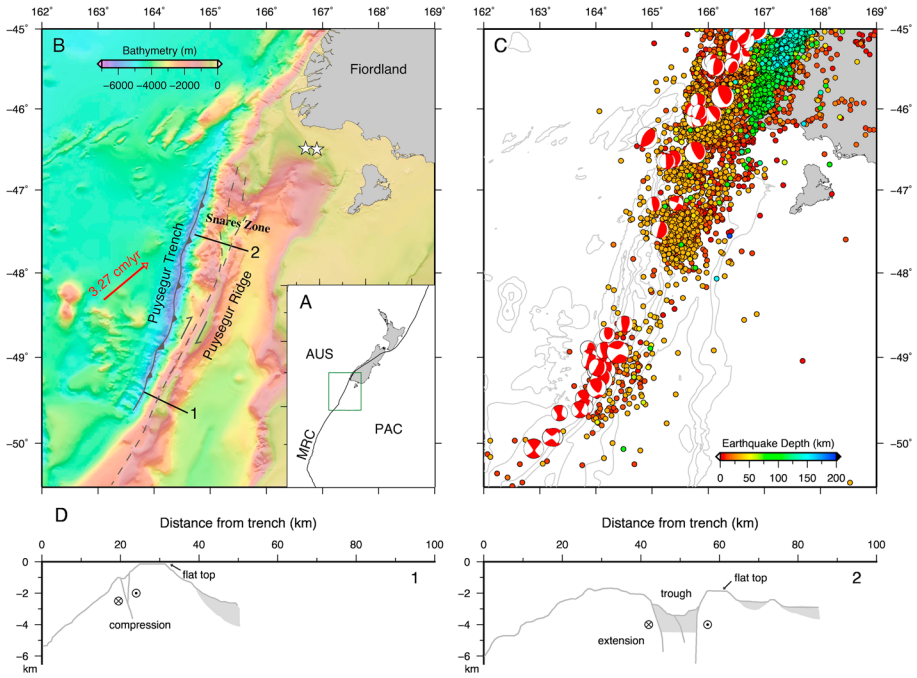

Figure 1. (a) Tectonic outline of the Puysegur region. AUS: Australian Plate; PAC: Pacific Plate; MRC: Macquarie Ridge Complex. (b) Bathymetry of the Puysegur Incipient Subduction Zone. The red vector is the relative velocity of AUS to PAC (DeMets et al., 1994). Stars show the location of young volcanic features (Sutherland et al., 2006), and black lines show position of cross sections in Figure 1d. Dashed lines show possible position of the Puysegur Fault. (c) Filled circles are earthquakes with magnitude between 2 and 5 from the ISC Bulletin (International Seismological Centre, 2014), and the focal mechanism solutions are from CMT catalog (Dziewonski et al., 1981). (d) Bathymetry cross sections and inferred fault structures (modified from Lebrun et al., 1998).

is largest and is roughly consistent with geodynamic models of induced subduction initiation (Gurnis et al., 2004). Discrete flat-topped segments, which are interpreted as the results of subaerial exposure and erosion, are also evident at both northern and southern parts of the Puysegur Ridge (Figure 1d). The southernmost segment is close to sea level (−120 m), while a peak subsidence of ~1800 m is found in the Snares Zone in the north, suggesting that the southern part has only experienced uplift, while there was uplift followed by subsidence in the Snares Zone (Collot et al., 1995; Gurnis et al., 2004; Lebrun et al., 1998). The width of the Puysegur ridge also widens northward from less than 50 km at 49.5°S to ~80 km at 47.5°S. A confined strike-slip fault zone is found near the peak of the ridge in the south, while a splayed fault zone structure is suggested in the trough of the Snares Zone (Figure 1d). Together, they show that the overriding plate close to the trench is under compression in the south and potentially in extension in the north (Collot et al., 1995; Lamarche & Lebrun, 2000). The corresponding trench depth in the south is about 1 km shallower than in the north (Collot et al., 1995). These spatial variations in structure along the PISZ are thought to represent different time periods in the evolution, and a space-for-time substitution can be made to compare the time evolution from 2-D models with the spatial variation along the PISZ.

The two-fault system at PISZ, with a thrust fault at the trench and a vertical fault inboard of the thrust fault, is recognized through the dual rupture mode for large earthquakes and interpretations of multibeam bathymetric, sonar imagery, seismic reflection, and geopotential data (Collot et al., 1995; Ruff et al., 1989). However, how this two-fault structure formed is still open to debate. Ruff et al. (1989) propose that the thrust interface formed through the propagation and connection of disconnected small thrust faults behind the vertical fault, while this hypothesis preceded the mapping of these two faults. Collot et al. (1995) propose that it developed through progressive adjustments of two adjacent vertical weak zones under compression, which requires the development of the ridge and differential uplift of the crustal block at one weak zone, and the rotation of the other. Here we propose that the two-fault system formed through developing a new thrust fault near the pre-existing vertical fault during subduction initiation. Previous studies suggest that there is a transition in the force balances from being forced externally to a state of self-sustaining subduction under its own negative buoyancy for induced subduction initiation (Gurnis et al., 2004; Leng & Gurnis, 2011). However, it is not clear

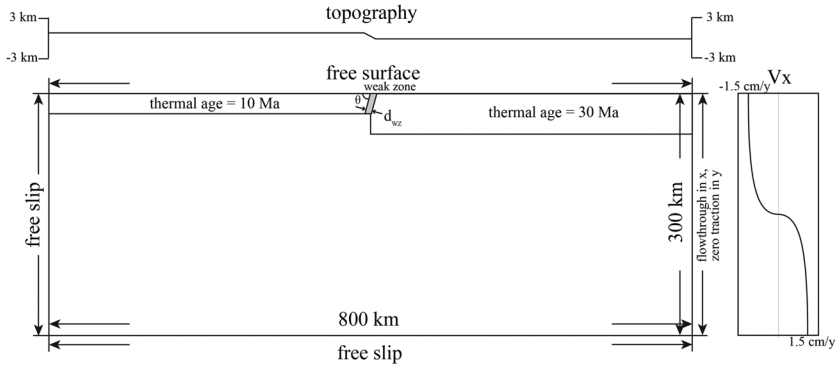

Figure 2. Model setup. The gray area shows the shape of the weak zone, with dip angle, θ, and width, d_{wz}. The weak zone is initialized with random plastic strain within 0–0.4, while other material properties remain unchanged. The finest resolution is 1 km × 1 km near the subduction zone, and the lowest is 3 km× 3 km in the asthenosphere.

whether PISZ is self-sustaining, or if the along strike variation in the uplift and subsidence of the Puysegur Ridge represents this transition. Here we use 2-D geodynamic models, which have a true free surface to track topographic changes, and model setup and boundary conditions tailored for PISZ, to test our hypothesis for the formation of the two-fault system at PISZ, and to explore the factors that control the transition in the force balance, while focusing on the evolution of topography and state of stress.

2. Method

Although a number of studies have tracked the topography in subduction zone models (e.g., Billen & Gurnis, 2001; Kaus et al., 2008; Gerya & Meilick, 2011; Zhong & Gurnis, 1994), predicting reliable topographic evolution in subduction zone remains a challenge. By reliable topography, we mean that not only is the predicted topography consistent with that observed but the model should also be able to include most of the important geophysical, petrological, and geochemical processes that affect the force balance, and the model setup, boundary conditions, and the evolution of material properties need to be self-consistent and properly constrained. During subduction initiation, the driving forces must overcome the resisting forces from the friction on the sliding interface, the bending of lithosphere and the buoyancy of oceanic crust (before the basalt-to-eclogite phase change) (e.g., McKenzie, 1977; Toth & Gurnis, 1998). With the subduction of the downgoing slab, phase changes in the crust lead to an increasing crustal density, and this part of the resisting force evolves to drive subduction. Fluids released from the subducting crust contribute to the decoupling between subducting and overriding plates, which may reduce the resisting force. Also influencing the force balance is the development of topography and surface process, which generate loads that affect lithospheric and mantle dynamics (Kaus et al., 2008, 2010).

A true free surface is tracked in pTatin3D (May et al., 2014, 2015), based on the Arbitrary Lagrangian Eulerian (ALE) finite element method, and is used to follow the dynamic mantle-surface interactions and the topographic evolution. Initial topography is calculated from isostasy (Figure 2), and topography is updated between time steps with surface velocity under the constraint that the vertical topographic change is smaller than 20 m to avoid topographic oscillation (Kaus et al., 2010). A simplified surface process model, based on linear topographic diffusion, is implemented (e.g., Avouac, 1996). A 5 km thick altered basaltic crust is placed on the top of dry pyrolite, and sediments are generated at the surface with our surface process. Density and free water content for different phase assemblages are gained by referring to precalculated 4-D (temperature, pressure, rock type, and total water content) phase maps using Perplex (Connolly, 2005). Darcy's law is used to migrate free water, and a linear water weakening is applied to the mantle material (Hirth & Kohlstedt, 1996). The Drucker-Prager yield criteria with a maximum yield stress are employed for material plasticity, and the accumulated plastic strain is recorded on tracers and used to reduce the material friction coefficient and cohesion. Elasticity alters the stress within the slab, and we include a new visco-elastic formulation called the Elastic Viscous Stress Splitting (EVSS) method (e.g., Keunings, 2000) in our model. Energy change with shear heating is treated as heat source terms and stored on tracers. Thermal and rheological parameters are given in Table S1 in the supporting information. More details on the numerical implementations of surface process, phase change, and EVSS are found in the supporting information.

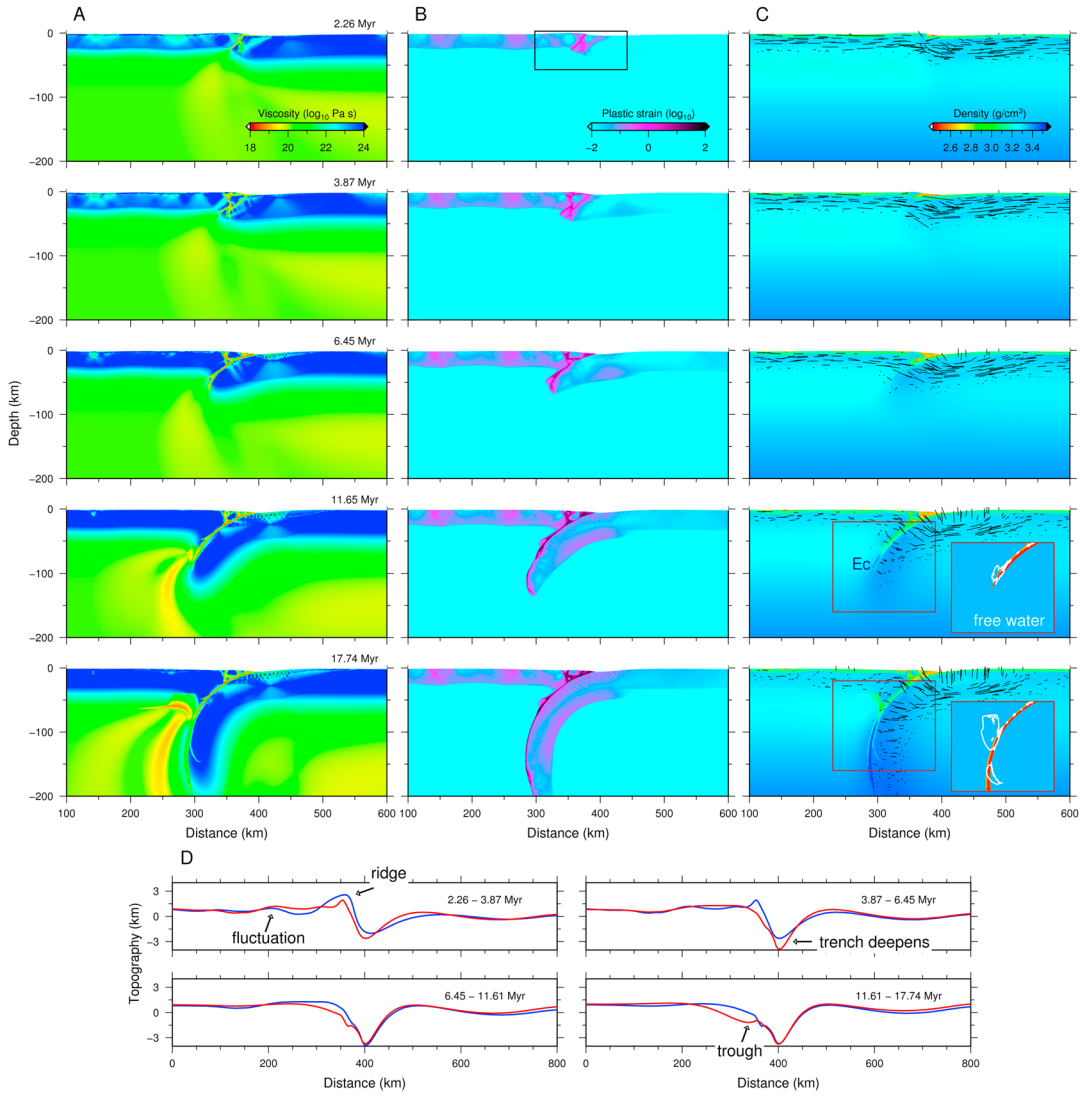

Figure 3. Model results (case SI1). (a) Effective viscosity evolution. (b) Accumulation of plastic strain. The black box shows the corresponding region for Figure 4a. (c) Density evolution. Black lines show direction and magnitude of maximum principal stress. Rock types and free water contents are shown in the insets with different colors and white contours. (d) Topography changes. Blue and red lines show initial and final topography for each time interval.

3. Results

We first show the detailed evolution of a subduction initiation case (SI1) that starts with a vertical weak zone with imposed far-field plate velocities (Figure 3), which are key aspects of PISZ. Initially (by 2.26 Myr), both the overriding and subducting plates are in a strong sense of compression, and the first lithospheric scale fault forms at the top of the initial weak zone with a high dip angle (fine structures shown in Figure 4a). Displacement on this new fault is small, and wide spread shear bands together with buckling of the lithosphere develop within the overriding plate. The buckling and shear bands absorb a considerable amount of the convergence. Some strain begins to localize at a shear band on the subducting plate side, and this shear band connects to the deeper part of the initial weak zone (Figure 4a). Responding to strong compression, a topographic pair of uplift adjacent to subsidence appear near the plate boundary at the overriding and subducting sides, respectively, and amplitudes of both are around 1.5 km (Figure 3d). Topographic fluctuation on the order of a hundred meters is predicted due to the lithospheric buckling in the overriding plate (Figure 3d). By 3.87 Myr, the shear band on the subducting plate side evolves into a new fault which later becomes the subduction interface. An ~30 km wide triangular lithospheric block which was on the subducting plate attaches to the overriding plate with the formation of the new plate boundary. A two-fault system,

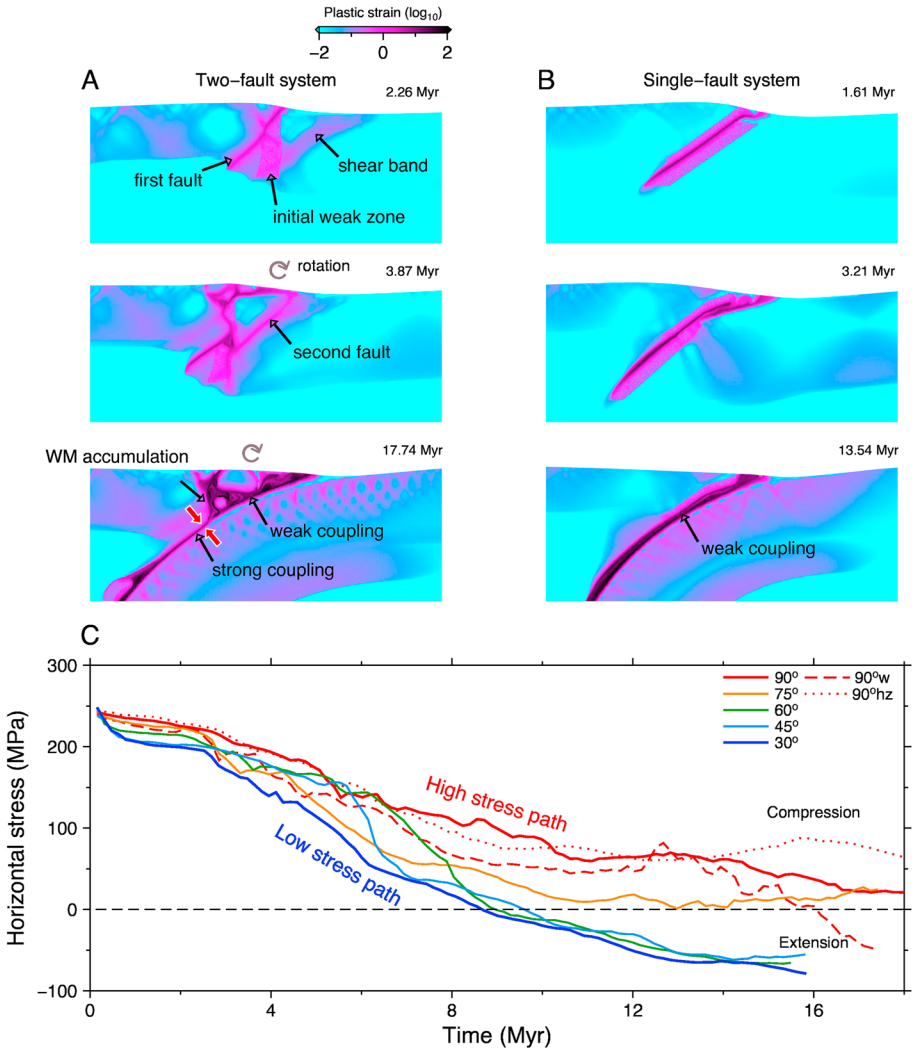

Figure 4. Model summary. (a, b) The zoomed-in plastic strains for cases SI1 and SI2, respectively. WM: weak material. (c) Averaged horizontal stresses within overriding plate for different cases. The averaging is performed within the region that spans from 100 km to 300 km distance and from surface to 25 km depth.

with the main thrust fault at the subduction interface and a vertical fault inboard of the thrust fault, starts to appear and dominate the deformation and structure of the overriding plate close to the trench. A sharp topographic signal is manifested with the uplift and rotation of the triangular block. The rough subduction interface is slowly smoothed by continuous tectonic erosion and plate bending from 3.87 to 11.65 Myr. With smoothing, the compressive stress in the overriding plate decreases (Figures 3c and 4c), and shear bands in the overriding plate become inactive (Figure 3a). Topography of the overriding plate close to the trench changes from uplift to subsidence, and the trench depth deepens (Figure 3d). The bending of the subducting plate causes near-surface extension and compression deeper within the subducting lithosphere near the trench, which leads to development of the forebulge topography and normal faults in the upper part of the lithosphere. Interestingly, these normal faults become temporarily inactive after they pass the bending region and enter the subduction zone (Figure 3a). Basalt transitions to eclogite at 70–80 km depth resulting in a density jump in the oceanic crust, and decoupling occurs between the overriding and subducting plates in the mantle wedge caused by released fluids. Both tend to bend the subducted slab to a higher dipping angle. A trough forms at the overriding plate close to the trench region when the slab reaches ~ 200 km depth (Figure 3d), and weak material consisting of sediments and crustal and lithospheric components (scrapped off along the interface) accumulates beneath the trough (Figure 4a).

We compare this case with one with a 30° dip angle weak zone (Figure S1). Initially, the subduction interface develops easily within the weak zone, and strain localizes to this thrust fault efficiently. The shape of the fault is favorable for subduction, and compression within the overriding plate decreases much faster compared to the case with a vertical weak zone. Only one fault develops during the entire subduction initiation process, and few shear bands appear during the early stage of compression. Lithospheric buckling of the overriding plate is absent in this case. The overriding plate close to the trench experiences uplift and subsidence during the initiation, while no trough-like structure develops. Unlike the vertical weak zone case, where the whole overriding plate is under weak compression or at a nearly neutral stress state after the smoothing of the subduction interface, the stress state in the overriding plate transitions into the extension phase quickly (Figure 4c).

To fill the gap between the two end-members of shallow and steep dipping weak zones, we computed three additional cases with dip angles of 45°, 60°, and 75° (Figures S2–S4). These models can be divided into two categories: one starts with high dip angles and evolves to a two-fault system (Figure 4a), while the other starts with a shallow dip and converges to a single-fault system (Figure 4b). During initiation, resisting forces in the two-fault system are at higher stress level, and the compression in the overriding plate can last much longer compared to the single-fault system (Figure 4c).

To test the other geometrical parameter that may influence the fault structure during subduction initiation, we conduct two more cases varying the width of the weak zone with a 90° dip angle (Figures S5 and S6). With a wider weak zone, the evolution pathway is generally similar to case SI1. The main differences are the triangular block between the thrust and vertical faults becomes smaller and the compressive stress within the overriding plate is at a slightly lower level. With half the width of the initial weak zone, the model fails to localize the deformation near the plate boundary. These two models confirm that once the weak zone is wide enough to localize the initial deformation, the dip angle plays a more important role to determine if a new fault is needed to initiate subduction.

In the previous cases, we focus on the influence of weak zone geometry on fault structure and stress state within the lithosphere during subduction initiation under compression, and we ignore a harzburgite layer in our density structure for simplicity (Figure S7). However, harzburgite has a slightly lower density compared to the undepleted mantle and could increase resisting forces for slab subduction (e.g., Arrial & Billen, 2013; Oxburgh & Parmentier, 1977). Therefore, we compare another case that incorporates a 15 km thick harzburgite layer beneath the crust (Figure S8) to case SI1 to test how this simplification affects our results. As we can see, these two cases give very similar model predictions on fault structure and topographic evolution (Figures 1 and S8), while the transition from compression to extension happens later with the addition of harzburgite (Figure 4c). This additional case suggests that during induced subduction initiation, early resistance mainly comes from friction on the plate interface and bending of the plates, while when slab approaches the transition threshold, positive buoyancy from chemical heterogeneities becomes important.

4. Discussion and Conclusion

Although the strike-slip motion on the Puysegur Fault is ignored in our 2-D model, our model predictions from case SI1 are generally consistent with field observations at PISZ. The uplift and subsidence of the topography on the overriding plate close to the trench agree with the uplift of the Puysegur Ridge in the south and uplift followed by subsidence in the north. The predicted trough has the similar distance to the trench as in the Snares Zone. The trench depth increase during the smoothing and maturation of the new thrust fault fits the depth difference between the southern and northern parts of the Puysegur Trench (~1,000 m). The buckling and shear bands that develop during the new fault formation are consistent with the renewed folding and reverse faulting on structures subparallel to the plate boundary on the overriding plate in the PISZ (Sutherland et al., 2006). More importantly, the predicted two-fault system, where a main thrust fault at the subduction interface and a vertical fault inboard of the thrust fault, is consistent with the Puysegur Trench and Fault structure.

Previous studies (Gurnis et al., 2004; Leng & Gurnis, 2011) suggest that the transition in the force balances from being forced externally to a state of self-sustaining subduction happens after a critical convergence is reached for induced subduction initiation, and the critical value is influenced by plastic parameters. Our results show that this transition is also affected by fault structures in two ways: one is through the development of the two-fault system, which absorbs some convergence and delays the transition, and the other is more

complex and related to the plate coupling difference between shallower and deeper parts. The rotation of the tectonic sliver between two faults causes the accumulation of weak materials beneath it, which results in a wider weak zone and a weaker plate coupling in the shallower part and a narrower weak zone and a stronger plate coupling in the deeper part. This coupling difference leads to a weak compression at the deeper part of the slab interface, which also contributes to a delay in the transition. We suggest that the PISZ may have not yet reached a state of self-sustaining subduction, and the subsidence at the overriding plate close to the trench may not be a direct proxy for the transition in the force balances. The Snares Zone may form through an isostatic response to tectonic erosion of a crustal root or pull by negative slab buoyancy, or both (Sutherland et al., 2006). Here we suggest that the opening of the trough maybe caused by the surficial extension resulting from the combined effects of the deeper compression between two plates and the rotation of the tectonic sliver. Our prediction of low-density material beneath the trough also helps to explain the strong (−110 mGal) localized low gravity anomaly at the Snares Zone, which is difficult to explain by subsidence alone (Lamarche & Lebrun, 2000).

In conclusion, our model motivated from the geological setting (Collot et al., 1995) requires a simpler initial condition, one weak zone instead of two, and gives more detailed explanation for the formation of the two-fault system at PISZ. Our model also provides important insights into how subduction initiates at fracture zones and transform faults, where the initial weak zone may have mechanically unfavorable dip angles.

Acknowledgments

X. M. and M. G. were supported by the National Science Foundation through awards EAR-1247022, EAR-1645775, and OCE-1654766. D. A. M. acknowledges financial support from the European Research Council under the European Union's Seventh Framework Programme (FP7/2007-2013)/ERC Grant Agreement 279925. Computations carried out on the NSF XSEDE systems, made possible by TG-EAR160027. We thank Magali Billen for her detailed review and constructive suggestions. Additional information for this article can be found in the supporting information. Source data for Figures 3 and 4 are available at https://doi.org/10.22002/D1.298.

References

Arrial, P.-A., & Billen, M. I. (2013). Influence of geometry and eclogitization on oceanic plateau subduction. *Earth and Planetary Science Letters*, *363*, 34–43.

Avouac, J.-P. (1996). Erosion as a driving mechanism of intracontinental mountain growth. *Journal of Geophysical Research*, *101*(B8), 17,747–17,769. https://doi.org/10.1029/96JB01344

Billen, M. I., & Gurnis, M. (2001). A low viscosity wedge in subduction zones. *Earth and Planetary Science Letters*, *193*(1), 227–236. https://doi.org/10.1016/S0012-821X(01)00482-4

Collot, J. Y., Lamarche, G., Wood, R. A., Delteil, J., Sosson, M., Lebrun, J.-F., & Coffin, M. F. (1995). Morphostructure of an incipient subduction zone along a transform plate boundary: Puysegur Ridge and Trench. *Geology*, *23*(6), 519–522. https://doi.org/10.1130/0091-7613(1995)023<0519:MOAISZ>2.3.CO;2

Connolly, J. A. D. (2005). Computation of phase equilibria by linear programming: A tool for geodynamic modeling and its application to subduction zone decarbonation. *Earth and Planetary Science Letters*, *236*(1), 524–541. https://doi.org/10.1016/j.epsl.2005.04.033

DeMets, C., Gordon, R. G., Argus, D. F., & Stein, S. (1994). Effect of recent revisions to the geomagnetic reversal time scale on estimates of current plate motions. *Geophysical research letters*, *21*, 2191–2194. https://doi.org/10.1029/94GL02118

Dziewonski, A. M., Chou, T.-A., & Woodhouse, J. H. (1981). Determination of earthquake source parameters from waveform data for studies of global and regional seismicity. *Journal of Geophysical Research*, *86*(B4), 2825–2852. https://doi.org/10.1029/JB086iB04p02825

Gerya, T. V., & Meilick, F. I. (2011). Geodynamic regimes of subduction under an active margin: Effects of rheological weakening by fluids and melts. *Journal of Metamorphic Geology*, *29*(1), 7–31. https://doi.org/10.1111/j.1525-1314.2010. 00904.x

Gurnis, M., Hall, C., & Lavier, L. (2004). Evolving force balance during incipient subduction. *Geochemistry, Geophysics, Geosystems*, *5*, Q07001. https://doi.org/10.1029/2003GC000681

Hirth, G., & Kohlstedt, D. L. (1996). Water in the oceanic upper mantle: Implications for rheology, melt extraction and the evolution of the lithosphere. *Earth and Planetary Science Letters*, *144*(1–2), 93–108. https://doi.org/10.1016/0012-821X(96)00154-9

International Seismological Centre (2014). *On-line bulletin*. Thatcham, UK: International Seismological Centre.

Kaus, B. J. P., Mühlhaus, H., & May, D. A. (2010). A stabilization algorithm for geodynamic numerical simulations with a free surface. *Physics of the Earth and Planetary Interiors*, *181*(1), 12–20. https://doi.org/10.1016/j.pepi.2010.04.007

Kaus, B. J. P., Steedman, C., & Becker, T. W. (2008). From passive continental margin to mountain belt: Insights from analytical and numerical models and application to Taiwan. *Physics of the Earth and Planetary Interiors*, *171*(1), 235–251. https://doi.org/10.1016/j.pepi.2008.06.015

Keunings, R (2000). Advances in the computer modeling of the flow of polymetric liquids. *Computational Fluid Dynamics Journal*, *9*(1), 449–458.

Lamarche, G., & Lebrun, J.-F. (2000). Transition from strike-slip faulting to oblique subduction: Active tectonics at the Puysegur Margin, South New Zealand. *Tectonophysics*, *316*(1), 67–89. https://doi.org/10.1016/S0040-1951(99)00232-2

Lebrun, J.-F., Karner, G. D., & Collot, J.-Y. (1998). Fracture zone subduction and reactivation across the Puysegur ridge/trench system, southern New Zealand. *Journal of Geophysical Research*, *103*, 7293–7313. https://doi.org/10.1029/98JB00025

Leng, W., & Gurnis, M. (2011). Dynamics of subduction initiation with different evolutionary pathways. *Geochemistry, Geophysics, Geosystems*, *12*, Q12018. https://doi.org/10.1029/2011GC003877

May, D. A., Brown, J., & Le Pourhiet, L. (2015). A scalable, matrix-free multigrid preconditioner for finite element discretizations of heterogeneous Stokes flow. *Computer Methods in Applied Mechanics and Engineering*, *290*, 496–523. https://doi.org/10.1016/j.cma.2015.03.014

May, D. A., Brown, J., & Le Pourhiet, L. (2014). pTatin3D: High-performance methods for long-term lithospheric dynamics, *Proceedings of the international conference for high performance computing, networking, storage and analysis* (pp. 274–284). New Orleans, LA: IEEE Press. https://doi.org/10.1109/SC.2014.28

McKenzie, D. P. (1977). The initiation of trenches. In M. Talwani, & W. C. Pitman (Eds.), *Island arcs, deep sea trenches and back-arc basins* (pp. 57–61). Washington, DC: American Geophysical Union. https://doi.org/10.1029/ME001p0057

Nikolaeva, K., Gerya, T. V., & Marques, F. O. (2010). Subduction initiation at passive margins: Numerical modeling. *Journal of Geophysical Research*, *115*, B03406. https://doi.org/10.1029/2009JB006549

Oxburgh, E. R., & Parmentier, E. M. (1977). Compositional and density stratification in oceanic lithosphere-causes and consequences. *Journal of the Geological Society*, *133*(4), 343–355.

Reay, A., & Parkinson, D. (1997). Adakites from Solander Island, New Zealand. *New Zealand journal of Geology and Geophysics*, *40*(2), 121–126. https://doi.org/10.1080/00288306.1997.9514746

Regenauer-Lieb, K., Yuen, D. A., & Branlund, J. (2001). The initiation of subduction: Criticality by addition of water? *Science*, *294*(5542), 578–580. https://doi.org/10.1126/science.1063891

Ruff, L. J., Given, J. W., Sanders, C. O., & Sperber, C. M. (1989). Large earthquakes in the Macquarie Ridge Complex: Transitional tectonics and subduction initiation. *Pure and Applied Geophysics*, *129*(1–2), 71–129.

Stern, R. J. (2004). Subduction initiation: Spontaneous and induced. *Earth and Planetary Science Letters*, *226*(3), 275–292. https://doi.org/10.1016/j.epsl.2004.08.007

Sutherland, R., Barnes, P., & Uruski, C. (2006). Miocene-Recent deformation, surface elevation, and volcanic intrusion of the overriding plate during subduction initiation, offshore southern Fiordland, Puysegur margin, southwest New Zealand. *New Zealand Journal of Geology and Geophysics*, *49*(1), 131–149. https://doi.org/10.1080/00288306.2006.9515154

Toth, J., & Gurnis, M. (1998). Dynamics of subduction initiation at preexisting fault zones. *Journal of Geophysical Research*, *103*(B8), 18,053–18,067. https://doi.org/10.1029/98JB01076

Thielmann, M., & Kaus, B. J. P. (2012). Shear heating induced lithospheric-scale localization: Does it result in subduction? *Earth and Planetary Science Letters*, *359*, 1–13. https://doi.org/10.1016/j.epsl.2012.10.002

Zhong, S., & Gurnis, M. (1994). Controls on trench topography from dynamic models of subducted slabs. *Journal of Geophysical Research*, *99*, 15,683–15,695. https://doi.org/10.1029/94JB00809